Electronic Supplementary Material (ESI) for Nanoscale.

Supplementary Information

InAs quantum dot in a needlelike tapered InP nanowire: a telecom band single photon source monolithically grown on silicon

Ali Jaffal,[*1a,b] *Walid Redjem,*[2] *Philippe Regreny,*[1b] *Hai-Son Nguyen,*[1b] *Sébastien Cueff,*[1b] *Xavier Letartre,*[1b] *Gilles Patriarche,*[3] *Emmanuel Rousseau,*[2] *Guillaume Cassabois,*[2] *Michel Gendry*[1b] *and Nicolas Chauvin*[1a]

[1]Université de Lyon, Institut des Nanotechnologies de Lyon, UMR 5270 CNRS,

[a]INSA de Lyon, 7 avenue Jean Capelle, 69621 Villeurbanne cedex, France

[b]Ecole Centrale de Lyon, 36 avenue Guy de Collongue, 69134 Ecully cedex, France.

[2]Université de Montpellier, Laboratoire Charles Coulomb, UMR 5221 CNRS, Place Eugène Bataillon, F-34095 Montpellier Cedex 5, France

[3]Université Paris-Saclay, Centre de Nanosciences et de Nanotechnologies, UMR 9001 CNRS,

10 boulevard Thomas Gobert, 91120 Palaiseau, France

Email : ali.jaffal@insa-lyon.fr

S1: TEM characterization of tapered NWs

S1.1: NWs with taper angle α ≈ 2°

TEM analysis on tapered InAs/InP QD-NWs have been performed to investigate the crystallographic properties of the NWs grown at T_G^{shell} = 420°C for 35 min with small taper angle α ≈ 2°, diameter D_{NW} = 360 nm and 14 µm in length (Figure 5a in the paper). Figure S1.1 (a) shows the two-beams dark-field TEM image of the upper of a typical NW. Although the bottom part of the NW is pure wurtzite (WZ), the upper tapered part is WZ with few stacking faults and short zinc blende (ZB) segments with a density in the order of 5-12 μm^{-1}. During the InP shell growth at 420°C, the WZ structure at the bottom part of the NWs is reproduced from the initial InAs/InP QD-NWs axially grown at 380°C. On the other hand, the stacking faults (Figure S1.1 (b)) and ZB segments at the upper part of the NWs appear during the axial growth that takes place simultaneously with the radial growth of the InP shell at 420°C.

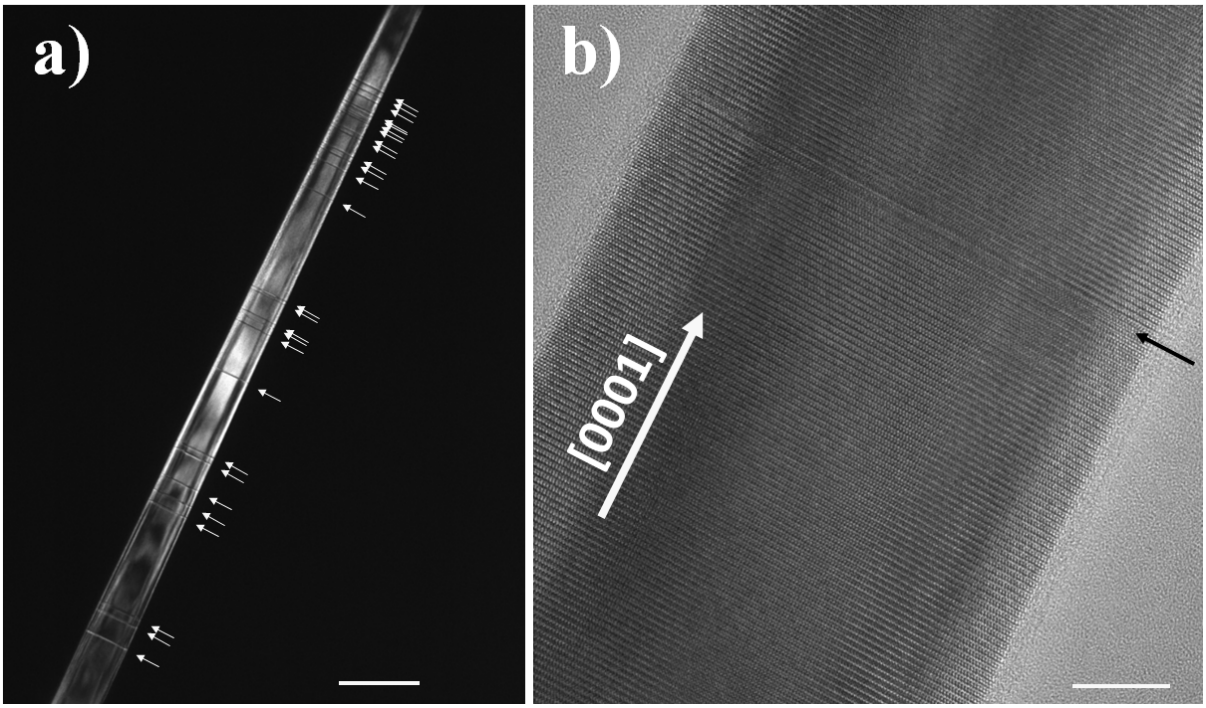

Figure S1.1. a) [1-100] dark-field TEM image of the upper part of the NW showing WZ structure with few structural defects such as stacking faults and ZB segments (indicated by white arrows). b) HRTEM image (in the [11-20] zone axis) showing a typical stacking fault in the WZ structure (indicated by the black arrow). Scale bars in (a) and (b) are 200 nm and 10 nm, respectively.

S1.2: NWs with taper angle α ≈ 7°

The stacking faults and the thin ZB segments at the upper part of the NW were eliminated using a lower T_G^{shell} = 380°C during 28 min (Figure 5b in the paper). With such growth conditions, the InAs/InP QD-NWs are shorter in length (4 µm) and have a wider taper angle α (7°) with similar D_{NW} = 370 nm, compared to the QD-NWs grown with T_G^{shell} = 420°C. Figure S1.2 (a,b) shows the two-beams dark-field TEM image of a typical NW and the HRTEM image in the [11-20] zone axis at the upper part of the NW, respectively. The crystal structure of such a QD-NW is defect-free from any stacking fault or ZB segment showing pure WZ crystal phase from the bottom to the upper part of the NW. The inset of Figure S1.2 (a) shows the diffraction pattern of the NW oriented in the [11-20] zone axis, confirming its pure WZ structure. This is explained by the used InP T_G^{shell} (380°C) which is similar to the axial growth temperature of the first InP stem corresponding to the optimal growth temperature for pure WZ

NWs. As a consequence, the WZ crystal phase was reproduced axially and radially during the growth stage of the InP shell at 380°C.

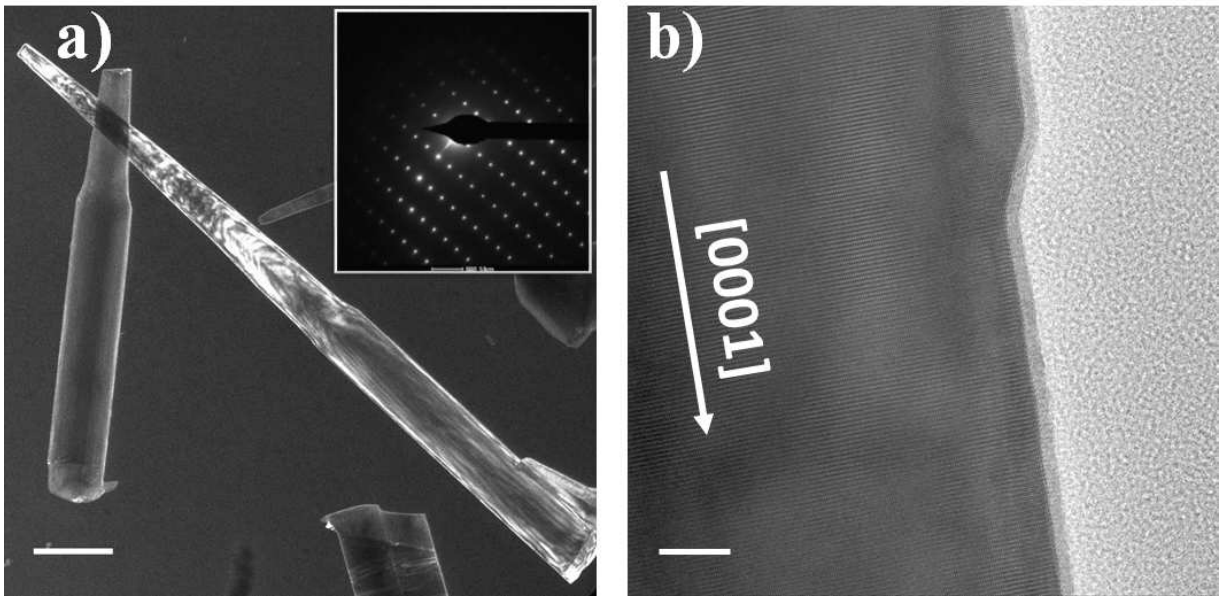

Figure S1.2. a) [1-100] dark-field TEM image showing the pure WZ structure along the total length of the NW. Inset is the diffraction pattern (in the [11-20] zone axis) of the NW. b) HRTEM image (in the [11-20] zone axis) at the upper part of the NW. Scale bars in (a) and (b) are 500 nm and 10 nm, respectively.

S2: Far-field setup

The schematic of the far-field setup is represented in Figure S2. Single QD-NWs are excited using a continuous 532 nm diode laser. The laser beam is expanded and coupled to a microscope objective (x50, numerical aperture NA = 0.8) by using a beam splitter. A 532 nm band pass filter is used. The light emitted from the QD is collected by the same microscope objective. The back focal plane of the objective contains the information of the emission directionality. Radiations emitted from the sample can be described as a superposition of plane waves, each defined by a unique wave vector (in reciprocal space). The objective lens focuses each individual plane wave into a spot with unique spatial coordinates at the back focal plane of the objective. In other words, the electric field distribution at the lens plane is Fourier transformed at the back focal plane. To have an image in real space, we use focusing lens (L2) to focus the QD emission on the InGaAs camera. A long pass filter (cut-on = 1300 nm) is used in order to cut the emission coming from the InAs/InP core-shell NWs and from the rough InP layer grown on the Si substrate allowing us to filter the QD emission only.

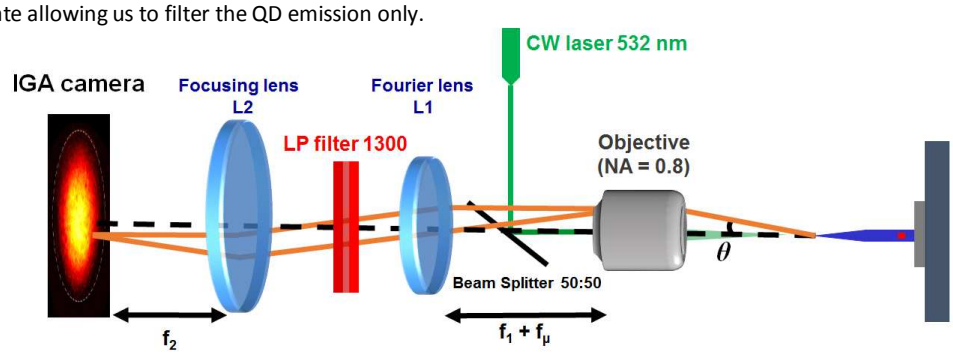

Figure S2. Schematic of the far-field setup.

S3: FDTD simulations

S3.1: Without a substrate: Effect of QD dipole orientation

FDTD simulations were performed as a function of the QD dipole orientation in order to understand the effect of the dipole orientation on the far-field emission profile. Figure S3.1 shows the calculated radiation pattern for a dipole oriented perpendicular (a) and parallel (b) to the NW axis. For the case of the dipole perpendicular to the NW axis, an excellent coupling takes place between QD dipole and the fundamental waveguide mode, HE_{11}, allowing efficient light collection from the NW top at small angle θ. The intensity of the calculated far-field emission is maximized at θ = 0 exhibiting a Gaussian radiation pattern for a perpendicular dipole. For the case of the parallel dipole, the far-field pattern's intensity is minimized at θ = 0. This is a direct evidence of the poor coupling between the parallel QD dipole and the HE_{11} mode of the NW. Therefore, the light emitted by the dipole propagates through non-guided leaky channels resulting in a non-Gaussian radiation pattern which is in agreement with previously reported studies.[1]

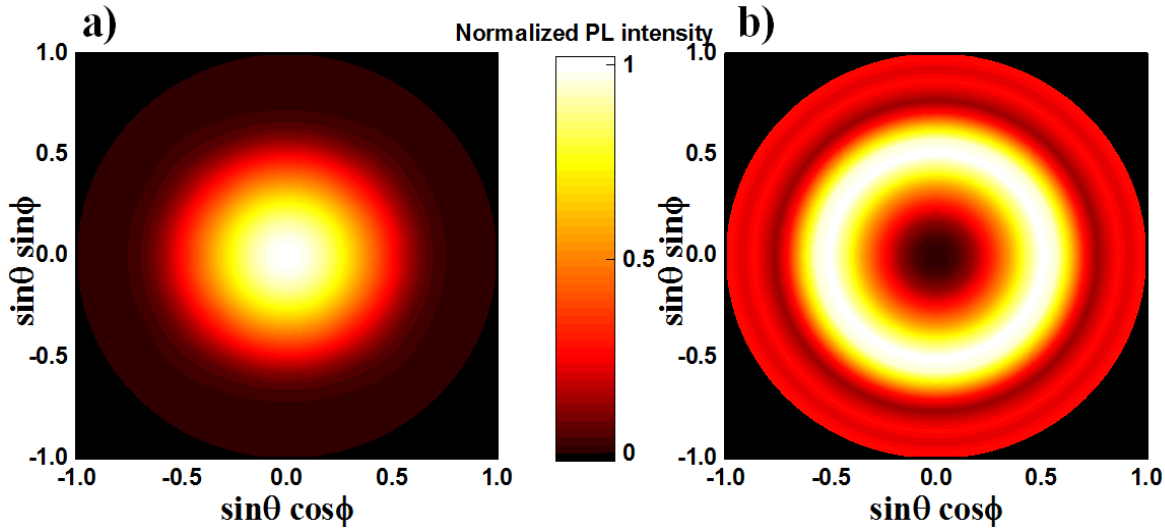

Figure S3.1. FDTD simulations of the emission profile in the far-field for a QD-NW without a substrate: a) QD dipole oriented perpendicular to the NW axis. b) QD dipole oriented parallel to the NW axis. The QD-NW is designed as a QD dipole emitting at 1.4 μm embedded in a tapered (α = 2°) cylindrical InP NW 320 nm in diameter equivalent to a 360 nm in diameter hexagonal NW. The PL intensity in (a) and (b) is normalized by the maximum of the intensity for each case.

S3.2: With a substrate:

The FDTD simulations presented in Figure 7a,b of the manuscript were performed assuming a semi-infinite NW to remove any back reflection of the guided mode as a consequence of the bottom NW/substrate interface. Figure S3.2 (a) shows the FDTD simulations for the case of a QD dipole oriented perpendicular to the NW axis where the NW is standing vertically on a flat InP substrate. An InP substrate was chosen for the simulations due to the presence of a rough 2D InP layer on the Si substrate after the growth of the QD-NWs. A strong modification in the radiation pattern of the InAs QD, in comparison with Figure S3.1a, takes place after the introduction of a substrate. The 2D cut along the emission profile in the direction of sinϕ = 0 is represented in Figure S3.2 (b). Although the radiation pattern is maximum at θ = 0, the Gaussian radiation pattern of the QD dipole is lost in this case. In a QD-NW waveguide system, 50% of the guided light goes upward whereas the other 50% goes downward.[2] As we have assumed a perfect flat substrate in our simulations, a partial reflection of the guided light going downward could occur at the NW/substrate interface and impact the radiation pattern. Such a radiation pattern has not been observed experimentally and we assume that the reflection of the guided mode in the bottom NW/InP layer interface is negligible due to the roughness of the layer.

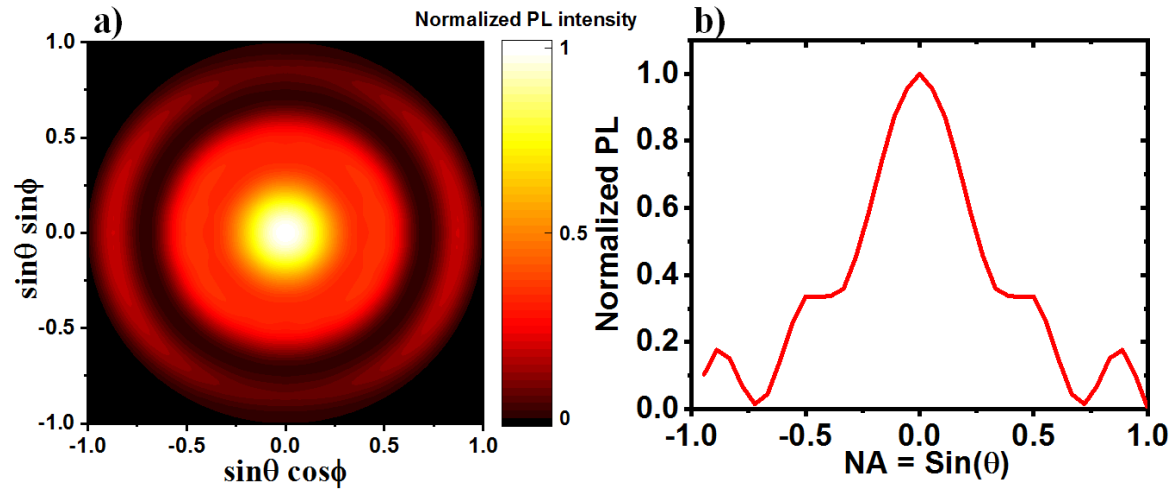

Figure S3.2. a) FDTD simulation of the emission profile in the far-field for a QD-NW with the same designed parameters as in Figure S3.1, but the QD-NW is standing vertically on an InP substrate. b) 2D cut along the calculated emission profile in (a) in the direction of sinϕ = 0. The PL intensity is normalized by the maximum of the intensity in (a) and (b).

S4: Effect of the NW diameter on the QD far-field emission profile

We have further studied the dependence of the QD emission profile in the far-field as a function of the NW diameter. Figure S4 shows the experimental emission profile of an InAs/InP QD-NW with a diameter D_{NW} = 360 nm (a) and D_{NW} = 480 nm (b). Both NWs have a taper angle α = 2°. In Figure S4a, the NW with D_{NW} = 360 nm corresponds to a single mode waveguide. The Gaussian far-field emission profile of the QD observed at this NW shows that a high fraction of the QD light couples to the HE_{11} mode of the NW. In contrast, the far-field emission profile of the QD for the NW with D_{NW} = 480 nm (Figure S4b) is broad compared to that one of Figure S4 (a) where the QD emission is collected at higher angles. This broadening in far-field profile is due to the QD coupling with higher order modes supported by the NW with D_{NW} = 480 nm.[2]

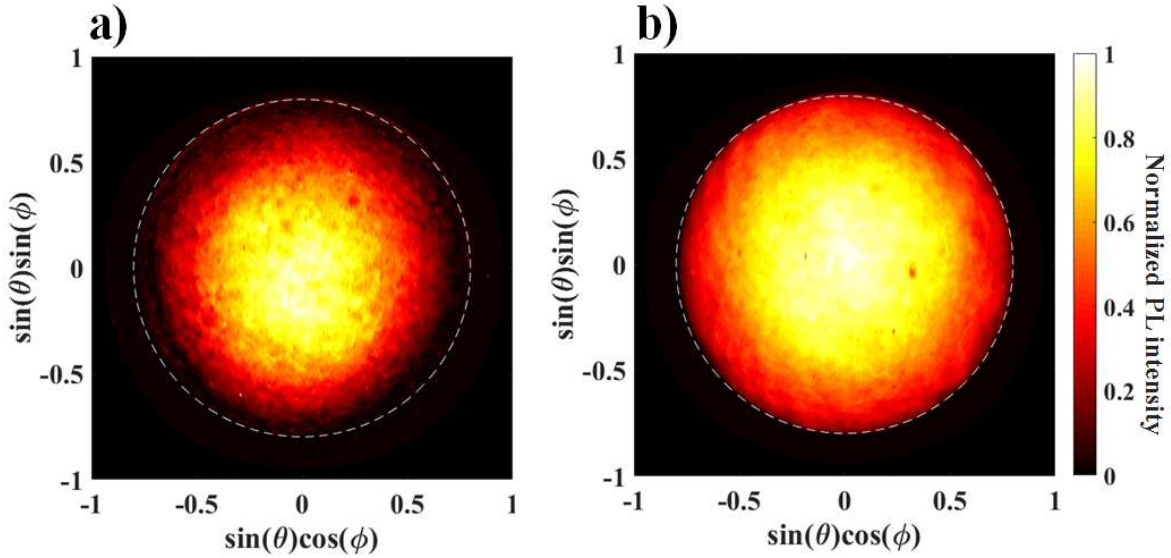

Figure S4. Experimental far-field emission profile at room temperature of a single InAs/InP QD-NW on a Si substrate. a) NW diameter D_{NW} = 360 nm, b) NW diameter D_{NW} = 480 nm. The PL intensity is normalized by the maximum of the intensity in (a) and (b) for each case. The dashed circle in (a) and (b) corresponds to the maximum collection of the numerical aperture.

S5: Auto-correlation measurements

We show in Figure S5 the micro-PL spectra of single InAs/InP QD-NWs emitting at 1256 nm (sample with 14 µm long NWs and α = 2°) (a) and at 1328 nm (sample with 4 µm long NWs and α = 7°) (b) that were used to perform corrections on the normalized $g_u^2(\tau)$ function. We consider that the peak from the QDs at 1256 nm and 1328 nm are the excitonic emission signals, S, and the rest is considered as background signals, B. The PL spectra were fitted by using a triple Lorentzian function in (a), a Gaussian function for the excitonic signal, S, and a triple Lorentzian function for the background signals B, in (b), in the 1250-1450 nm spectral range corresponding to the same range of the auto-correlation measurement. Then, the S to B ratio was calculated using the equation: ρ = S/(S+B) resulting in ρ = 0.84 in (a) and ρ = 0.76 in (b). The uncorrected $g_u^2(\tau)$ function was corrected using the equation $g^2(\tau)-1= (g_u^2(\tau)-1)/\rho^2$.

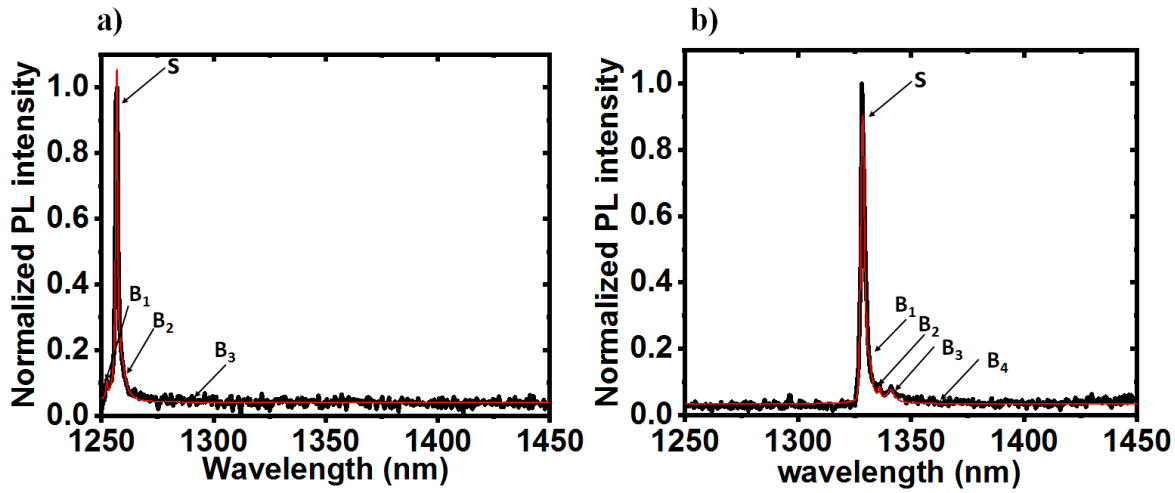

Figure S5. micro-PL spectra of a single InAs/InP QD-NW from: a) 14 µm-length QD-NW with α = 2° emitting at 1256 nm (987 meV), b) 4 µm-length QD-NW with α = 7° emitting at 1328 nm (933 meV). The solid red lines are triple Lorentzian fit in (a) and Gaussian fit for the excitonic signal and triple Lorentzian fit for the background signals in (b).

References:

1 G. Bulgarini, M. E. Reimer, M. Bouwes Bavinck, K. D. Jöns, D. Dalacu, P. J. Poole, E. P. A. M. Bakkers and V. Zwiller, *Nano Lett.*, 2014, **14**, 4102–4106.

2 I. Friedler, C. Sauvan, J. P. Hugonin, P. Lalanne, J. Claudon and J. M. Gérard, *Opt. Express*, 2009, **17**, 2095–110.